Plasmon-enhanced downshifting and downconversion: Fundamentals and applications in photovoltaics

Aditi Joshi [a,b], Ilia L. Rasskazov [b,*]

[a] *School of Mathematics and Statistics, Rochester Institute of Technology, Rochester, NY 14623, USA*
[b] *SunDensity Inc., Rochester, NY 14604, USA*

A B S T R A C T

Downshifting (DS) and downconversion (DC) are processes in which a high-energy photon is converted into one or several lower-energy photons, respectively. These processes have potential applications in imaging, solar energy harvesting, color conversion, and other fields. The quantum efficiency of DS and DC can be high, even surpassing 100%. However, efficient photon management is crucial for most applications, and improving the yield of DS and DC is highly desirable. One promising and relatively easy way to boost the yield of DS and DC is to utilize plasmonic nanoparticles. The resonant electric field enhancement near plasmonic nanoparticles leads to an increased excitation rate of DS and DC. However, the presence of metallic nanoparticles quenches the emission at both micro and macro scales due to Ohmic losses. Properly balancing enhancement and quenching by choosing the optimal shape, material, size, and concentration of plasmonic nanoparticles has been shown to boost DS and DC by a factor as large as 50×. In this review, we discuss the basics of plasmon-enhanced DS and DC and highlight recent progress in this field, covering experimental demonstrations of this concept and its implications for photovoltaics.

Contents

1. Introduction

The concept of splitting an ultraviolet (UV) photon into two visible photons, a process that effectively harnesses the energy of high-frequency photons to generate a pair of lower-frequency photons, was first proposed by Dexter in 1957 [1]. This groundbreaking idea laid the foundation for what would later be known as downconversion (DC), sometimes referred as to "quantum cutting", a

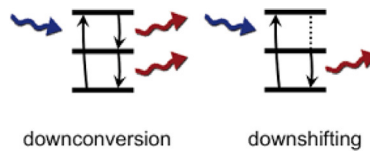**Fig. 1.** Simplified energy diagrams of downconversion (DC) and downshifting (DS).
Source: Reproduced from Ref. [14].

phenomenon that is the opposite of the upconversion process, or "Addition de Photons par Transfert d'Energie", discovered by Auzel in 1966 [2]. The first experimental observations of downconversion were reported independently by two research groups in 1974, using YF_3^{3+} as the material system [3–5]. Subsequent advancements in the field led to significant milestones, such as the demonstration of nearly 200% quantum yield in Eu^{3+}-doped $LiGdF_4$ through partial energy transfer between ions [6–8], which immediately promoted the practical importance of DC.

Similarly, downshifting (DS) involves the absorption of higher-energy photons (such as ultraviolet or blue light) by a luminescent material, followed by the emission of photons at longer wavelengths (lower energy), typically in the visible spectrum. The key difference between DS and DC lies in the fact that DS results in the emission of only one photon, whereas DC results in the emission of many, as illustrated in Fig. 1. Both DS and DC have found extensive applications in various fields, including bioimaging [9], optoelectronics [10], and solar energy harvesting [11–13]. Despite the relatively high efficiencies already achieved in DS and DC processes, there is a consistent challenge and ongoing effort to further improve their performance. Even incremental enhancements in DS and DC efficiencies can have far-reaching consequences. For instance, in solar modules, slightly higher DS and DC efficiencies of utilized luminescent materials may lead to substantially larger energy yield at large industrial scale.

Numerous strategies have been explored to enhance DS and DC processes. These include integrating metal–organic frameworks [15] or nonlinear crystals [16] into DS/DC systems. Another approach is dye-sensitization, where dye molecules are used to absorb light and transfer energy to the luminescent material, thereby enhancing the DC process [17]. Additionally, introducing defects into the crystal structure of DS/DC materials has been shown to improve their performance by distorting crystal field [18]. Among these approaches, the use of plasmonic nanoparticles (NPs) has emerged as a particularly promising and extensively studied avenue for enhancing DS and DC processes. The emergence of localized surface plasmon resonance (LSPR) in plasmonic NPs can significantly enhance the electromagnetic field around the particles, leading to increased light absorption and emission by nearby luminescent material. Plasmonic NPs are commercially available, relatively easy to handle, and exhibit strong resonances in the UV–Vis wavelength range, which makes them especially attractive to use in DC and DS processes.

This review aims to provide a comprehensive overview of the current state of the art in plasmon-enhanced DS and DC, focusing on fundamental principles, experimental demonstrations, and photovoltaic applications. In Section 2, we explore theoretical frameworks that describe the interaction of plasmonic NPs with light and luminescent materials, including LSPR and luminescence decay rates. In Section 3, we present experimental demonstrations highlighting the potential of plasmon-enhanced DS and DC, covering various types of plasmonic NPs and their integration with luminescent materials. We discuss the impact of NP size, shape, and composition on DS/DC enhancement. Finally, in Section 4, we overview the most representative examples of plasmon-enhanced DS and DC in photovoltaics, examining how these processes can convert high-energy photons into usable energy, benefiting various solar cell technologies. By assessing the current state of the art, we conclude with insights into future research directions and the potential for optimizing DS and DC processes through plasmonic enhancement.

2. Plasmon-enhanced downshifting and downconversion

LSPRs are collective oscillations of free electrons in metal NPs of the size smaller or comparable with the free electron path. LSPRs originate if the electric field penetrates the metal and causes displacement of electrons with respect to the lattice resulting in the opposite charges appearing at the opposing surfaces. The attraction of these charges causes a restoring force that along with the (effective) mass of the electrons defines an electromechanical oscillator called a surface plasmon. When the frequency of surface plasmon is close to the frequency of the excitation light wave, LSPR occurs which leads to the enhanced local field at the surface. For spherical particle, within quasistatic approximation, the wavelength of the resonance can be identified at $\Re(\varepsilon) = -2\varepsilon_h$, where ε and ε_h are permittivities of NP and the host, respectively. LSPRs have been heavily studied in conjunction with a large amount of applications. Interested reader is referred to seminal reviews and tutorials [22–27] including applications in photovoltaic devices [28], nonlinear optics [29], nanolasers [30] and recent trends in understanding peculiar features of ultra-fine plasmonic NPs [31]

Fig. 2 summarizes optical properties of three plasmonic materials most commonly used in DS and DC: Al, Ag and Au. Within the quasistatic approximation, an anticipated wavelength of LSPR of NPs embedded in the glass host with $\varepsilon_h = 2.25$ broadly varies from UV for Al to visible for Au, see Fig. 2(a)–(c). These trends can be further confirmed by solving rigorously the electromagnetic problem of planewave incident on a sphere [32]. The most straightforward way to assess the resonant behavior of NP is through its extinction spectra which characterizes how effectively NP removes light from an incident beam through both scattering and absorption processes. Explicit expressions for the extinction efficiency, Q_{ext}, can be found elsewhere [33]. Rigorous calculations of Q_{ext} presented in Fig. 2(d)–(f) show that indeed, extinction efficiency of NPs acquires maximum values from UV for Al to visible
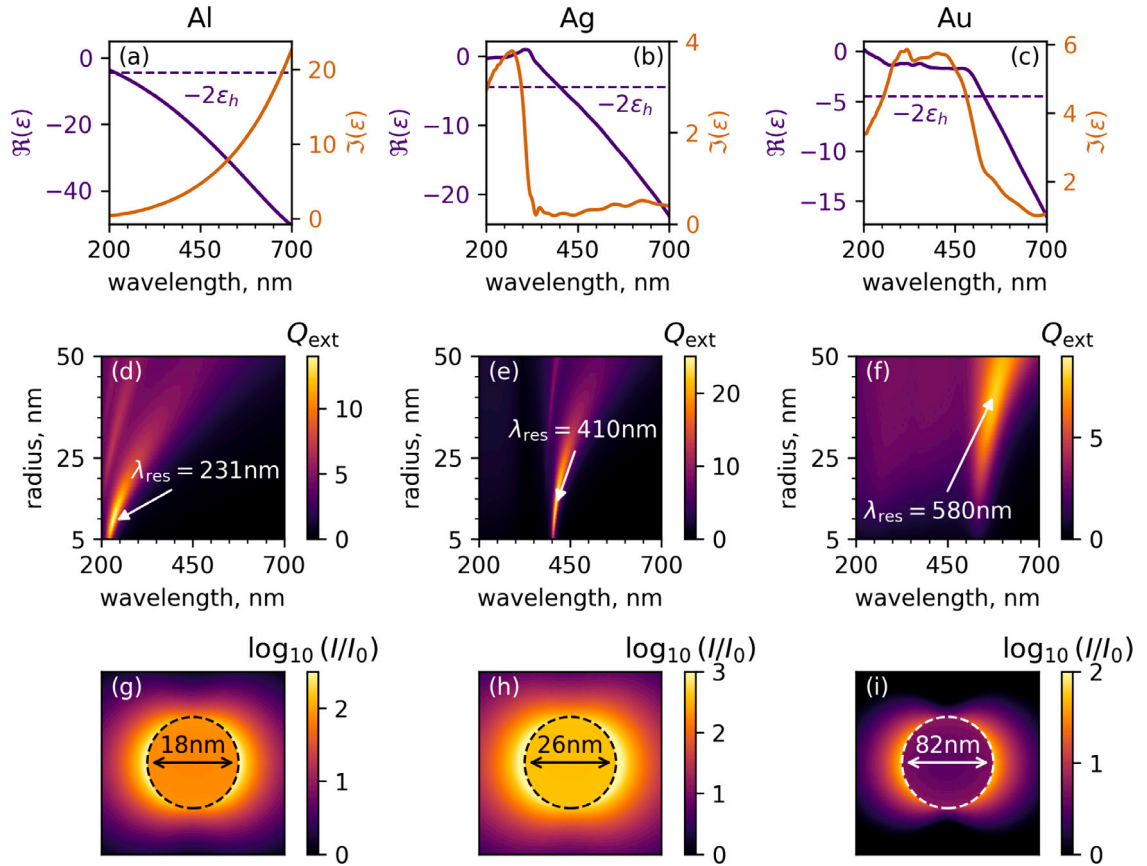
Fig. 2. Real and imaginary dielectric functions of (a) Al [19], (b) Ag [20], (c) Au [20]. Horizontal dashed lines in (a)–(c) correspond to $-2\varepsilon_h$, where in our case $\varepsilon_h = 2.25$ (typical glass). Extinction efficiency for (d) Al, (e) Ag, and (f) Au spheres of different radius as a function of vacuum wavelength of incident light. Arrows in (d)–(f) point to maximum achievable Q_{ext} within a given range of parameters. (g)–(i) Normalized electric field intensity, I/I_0, inside and near NPs for sizes and at wavelength highlighted in plots (d)–(f) and corresponding to maximum Q_{ext} indicated with arrows. Simulations presented in panels (d)–(i) are performed via the open-source MATLAB code STRATIFY [21] utilizing dielectric functions for Al, Ag and Au as presented in panels (a)–(c).
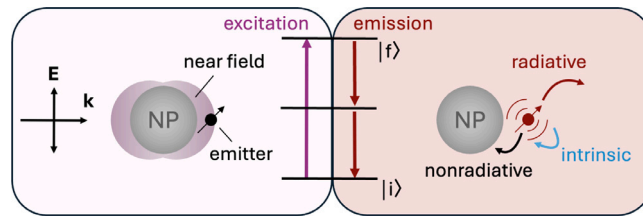
Fig. 3. Simplified schematic representation of plasmon-enhanced DC in a presence of plasmonic NP. *Excitation* process represents plane wave incident into the NP-emitter system, consequent strong local field enhancement in the vicinity of NP in case of wavelength of incident illumination coinciding with the LSPR wavelength of NP and increased excitation rate of the emitter (according to Eq. (1)) located in the spot with large electric field intensity. In the *emission* process, emitter can be considered as an electric dipole oscillating in a presence of a metallic sphere. Notice the absence of external plane wave illumination in this case. Plasmonic NP simultaneously modifies radiative decay rates at wavelength corresponding to LSPR and increases nonradiative decay rates of the emitter due to Ohmic losses.

for Au NPs of typical radius from 5 nm to 50 nm, which is associated with the emergence of LSPR. Fig. 2(g)–(i) further elaborates on properties of LSPRs: electric field confinement appears to be exceptionally strong near the surface of nanospheres. The latter property allows to manipulate excitation and emission of the emitter located near plasmonic NP. According to Fermi's golden rule, the transition rate γ_{exc} of photons corresponding to the excitation of DS/DC emitter from $|i\rangle$ to $|f\rangle$ state is proportional to the intensity of the electric field at the location of the emitter (see Fig. 3):

$$\gamma_{exc} = \frac{2\pi}{\hbar} |\langle f |\mathbf{E} \cdot \mathbf{p}| i \rangle|^2 \rho_f , \tag{1}$$

where $\hbar$ is the reduced Plank's constant, $\mathbf{E}$ is the electric field at the emitter location, $\mathbf{p}$ is the transition dipole moment, and ρ_f is the density of final states.

At the same time, radiative, Γ_{rad}, and, more importantly, nonradiative, Γ_{nrad}, decay rates of transitions associated with the emission of the emitter are modified in the presence of plasmonic NP. In this case, quantum yield of emitter–NP system reads as:

$$q = \frac{\tilde{\Gamma}_{\text{rad}}}{\tilde{\Gamma}_{\text{rad}} + \tilde{\Gamma}_{\text{nrad}} + (1 - q_0)/q_0} \ . \tag{2}$$

Here q_0 is quantum yield of the emitter for a single-photon transition in the absence of NP, the term $(1-q_0)/q_0$ describes the intrinsic decay rates associated with internal non-radiative channels, which is typically assumed to be unaffected by plasmonic NP. Tilde over decay rates $\tilde{\Gamma}_{\text{rad(nrad)}}$ denotes normalization of decay rates to that of in free space, i.e. in the absence of plasmonic NP. Noteworthy, decay rates of the emitter are dependent on the orientation of the dipole moment $\mathbf{p}$ with respect to NP. In rare occasions, well-defined orientation of $\mathbf{p}$ can be realized, while in most of the cases, orientation-averaging has to be implemented. For example, in the case of emitter located near spherical NP, orientation-averaged decay rates are: $\tilde{\Gamma}_{\text{rad(nrad)}} = \left(\tilde{\Gamma}_{\text{rad(nrad)}}^{\perp} + 2\tilde{\Gamma}_{\text{rad(nrad)}}^{\parallel} \right)/3$, where $\perp$ and $\parallel$ denote the dipole oriented perpendicular and parallel to the surface of a sphere.

Ultimately, the DS or DC enhancement factor is defined as a product of excitation enhancement and quantum yield modification:

$$F = \frac{\gamma_{\text{exc}}}{\gamma_{\text{exc;0}}} \times \left(\frac{q}{q_0} \right)^p \ , \tag{3}$$

where $\gamma_{\text{exc;0}}$ is the transition rate of photons corresponding to the excitation of DS/DC emitter in the absence of NP, and p is the number of photons emitted: $p = 1$ for DS and $p > 1$ for DC.

Generally speaking, the validity of Eqs. (1)–(3) has been demonstrated for metal-enhanced fluorescence ($p = 1$ in this case) in seminal experiments [34,35] for Nile Blue dye in a presence of Au NP. DS, being in fact the same as fluorescence, can be described by similar approach, while DC, involving several emitted photons, requires $p > 1$ for the second term in Eq. (3).

Several important features of plasmon-enhanced DS/DC worth separate discussion:

- There are no new photons generated during plasmon-enhanced excitation process, it is a transition rate increased according to Eq. (1).
- Enhancement factors F calculated via Eq. (3) strongly depend on q_0. The worse emitter is used (i.e. with low q_0), the larger F can be achieved upon using the same plasmonic NP, given that excitation and emission spectra do not change, see for example a detailed discussion on the example of plasmon-enhanced fluorescence [36].
- For a *suspension* of plasmonic NPs, attenuation of electromagnetic wave at the macro-scale occurs due to Ohmic losses in metal. This effect is not captured by Eq. (3) which is valid for the case of a *single* NP. Competition between locally enhanced DS/DC and its attenuation at macro-scale requires careful optimization of concentration of NPs, which has been demonstrated in several works [37–40], but without proper theoretical background. Similar competition between plasmon enhancement at nano-scale and attenuation at macro-scale has been demonstrated for plasmon-enhanced surface enhanced Raman spectroscopy [41], stimulated Raman [42,43], and upconversion [44]. This effect should not be confused with so-called *concentration quenching*, where "concentration" is referred to the concentration of emitters [45].
- Rare-earth ions, widely used for DS and DC, emit light at multiple wavelengths with different intensities [46–49]. Apart from sole enhancing DS/DC, it might be important to control branching ratio of different emission channels [50].
- It may not be obvious immediately, but *the very nature of the electric field enhancement is not important at all* for boosting excitation rate γ_{exc} in Eq. (1). Any other approach for enhancing local electric field other than using plasmonic NPs will do the trick. For instance, work [18] demonstrates 10.64x four-photon near-infrared DC enhancement in $NaBaPO_4$:Er^{3+} phosphors due to the distortion of local crystal field by co-doping Bi^{3+} into $NaBaPO_4$:Er^{3+}.

Interestingly, specific to DS and DC, the very effect of modification of decay rates, and, as a consequence, quantum yield and Purcell factor by plasmonic NP, has been addressed numerically only in one recent work [51]. Moreover, only a small fraction of works on plasmon-enhanced DS and DC present near-field calculations for plasmonic NPs under consideration [40,51–57]. That said, we can allude that theoretical understanding of plasmon-enhanced DS and DC processes, even being similar to well-established plasmon-enhanced fluorescence [58,59] or upconversion [60–63], appears to be immature.

3. Experimental demonstrations of plasmon-enhanced downshifting and downconversion

There are multiple strategies for combining together plasmonic NPs and DS/DC materials for plasmon-enhanced DS/DC as demonstrated in Fig. 4 with more detailed information available in Table 1. Pioneering works demonstrated the effect of plasmonic enhancement by embedding both DS emitters and plasmonic NP in glass-like host [64,67,68,72] or solution [73,75]. Alternatively, plasmonic NPs can be mixed with phosphors [39,53,69,76,77] or located on their surfaces [40,82]. Another sophisticated approaches ensuring effectiveness of plasmonic enhancement include targeted positioning of DS/DC emitters/NPs directly on the surface of plasmonic NPs [37,52,80] or *vice versa*, DS NPs can be decorated with plasmonic NPs [70,74,79,81]. More complex arrangements of plasmonic NPs and DS/DC emitters are: films with composite plasmonic/DS NPs [38], SiO_2 microspheres decorated with plasmonic Ag NPs surrounded by silica with CdZnSeS QDs [66], inverse opals [78], periodic [54,56,57] and disordered [55,65,71] arrays of plasmonic NPs with DS/DC emitters attached to them.
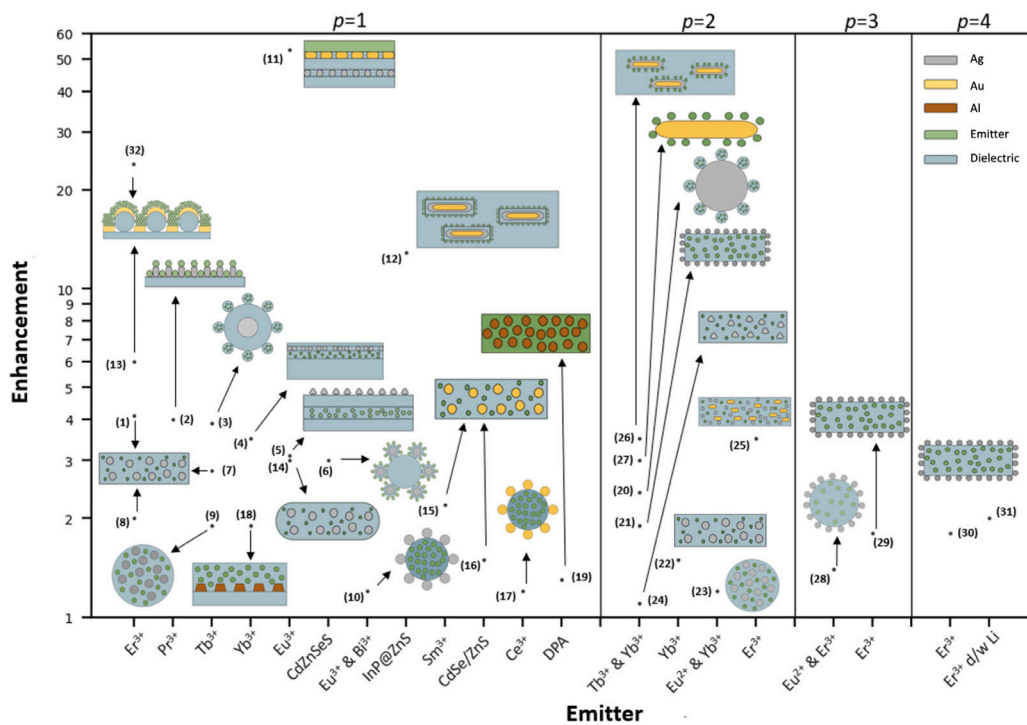
Fig. 4. Experimentally measured DS and DC enhancements (in logarithmic scale) due to plasmonic effects of various nanostructures with respective schematic sketches of their arrangements for different types of emitters and number of emitted photons, p (see Table 1 for more details): **(1)** Zinc-boro-tellurite glass:Er^{3+} containing Ag NPs [64], **(2)** Ag nanopillar array with spin coated β-NaYF4:Pr^{3+} NPs [54], **(3)** Ag@SiO$_2$ nanospheres with attached ligand-free β-NaYF4:Tb^{3+} NPs, in water solution [37], **(4)** YAG substrate, YAG:Ce^{3+},Yb^{3+} phosphor layer covered with SiO$_2$ spacer, Ag NPs, and SiO$_2$ passivation layer [55], **(5)** GdVO$_4$:Eu^{3+}, PVA and Ag nanoprism layers on Si cell surface [65], **(6)** SiO$_2$ microspheres decorated with plasmonic Ag NPs surrounded by silica with CdZnSeS QDs [66], **(7)** Tb^{3+} and Ag co-doped glass nanocomposites synthesized in Li$_2$O-LaF$_3$-Al$_2$O$_3$-SiO$_2$ glass matrix [67], **(8)** Er^{3+}-doped Ga$_{10}$Ge$_{25}$S$_{65}$ glass containing Ag NPs [68], **(9)** Ag co-doped Y$_2$O$_3$:Tb^{3+} [69], **(10)** YVO$_4$:Eu^{3+},Bi^{3+} NPs decorated with Ag NPs [70], **(11)** Eu^{3+}/Au nanorods/PMMA spacer layer/Ag NPs/ glass [71], **(12)** Au@Ag@SiO$_2$ NPs and InP@ZnS QDs in PLMA [38], **(13)** NaGdF$_4$:Yb^{3+},Er^{3+},Ce^{3+}@NaGdF$_4$,Nd@NaGdF$_4$ core–shell–shell downconversion NPs and Au hole-cap nanoarray on PS self-assembled film [57], **(14)** Ag/La$_{0.95}$Eu$_{0.05}$PO$_4$ nanostructures [39], **(15)** Sm^{3+}-doped sodium tellurite glass embedded with Au NPs [72], **(16)** CdSe@ZnS QDs and Au NPs dispersed in epoxy resin [73], **(17)** Au-YAG:Ce^{3+} composite [74], **(18)** Al nanocylinder arrays structured on SiO$_2$ glass substrate with CaF$_2$:Yb^{3+},Er^{3+} NPs layer placed onto the array [56], **(19)** Al NPs dispersed in DPA [75], **(20)** β-NaYF$_4$:Tb^{3+},Yb^{3+} NPs doped with Ag NPs [52], **(21)** NaBaPO$_4$:Eu^{2+},Yb^{3+} decorated with Ag NPs [76], **(22)** KYF$_4$:Tb^{3+}, Yb^{3+} doped Ag NPs [77], **(23)** Ag co-doped Y$_2$O$_3$:Yb^{3+} [69], **(24)** NaYF$_4$:Tb^{3+},Yb^{3+} NPs decorated with triangular Ag NPs [78], **(25)** β-NaYF$_4$:Er^{3+} NPs decorated with the Ag nanocubes and Au nanorods [79], **(26)** Au@SiO$_2$ nanorods combined with NaYF$_4$:Tb^{3+},Yb^{3+} NPs in water solution [80], **(27)** β-NaYF$_4$:Tb^{3+},Yb^{3+} NPs decorated with Au nanorods [53], **(28)** NaBaPO$_4$:Eu^{2+},Er^{3+} decorated with Ag NPs [81], **(29)** and **(30)** NaBaPO$_4$:Er^{3+} decorated with Ag NPs [82], **(31)** NaBaPO$_4$:Er^{3+},Li^+ decorated with Ag NPs [40]. **(32)** NaYF$_4$:Yb^{3+},Er^{3+},Ce^{3+} downconversion NPs and Ag hole-cap nanoarray on PS self-assembled film [51].

So far, only three metals have been extensively used for plasmon-enhanced DS/DC: Al, Ag and Au. Several works also considered simultaneously Au and Ag NPs [71,79] and composite Au@Ag core–shell NPs [38]. Only two experimental works [38,71], which in fact use a combination of Ag and Au NPs, report enhancement factor surpassing 10×. Interestingly, Al NPs, being well known for extraordinary plasmonic properties in UV–visible range [85–87], are only suggested in two works for plasmon-enhanced DS [56,75] to date. Alloy and multimetallic NPs [88–94] along with recently emerged and promising plasmonic Mg NPs [95,96] are yet to be considered for DS/DC enhancement.

Fig. 5 demonstrates the most representative example of plasmon-enhanced DS reported in Ref. [71]. Several features are worth discussion here:

- Both excitation and emission spectra of the emitter are boosted in a presence of NPs as seen in Fig. 5(a),(b). The excitation is increased due to the increased absorption in a presence of NPs, while the emission is increased due to lager amount of photons emitted by the emitter.
- The ratio between photons emitted with and without presence of NPs then ultimately yields the enhancement factor plotted in Fig. 5(c).
- Enhancement factor strongly depends on concentration of plasmonic NPs with a pronounced maximum of the enhancement at a certain concentration, Fig. 5(c). As discussed above, this observation can be well explained by the interplay between local enhancement of the DS process via plasmonic NP and quenching of the enhanced signal due to increased absorption inevitable for higher concentrations of plasmonic NPs. We emphasize that similar existence of the optimal concentration of plasmonic NPs has been theoretically predicted and experimentally observed for surface enhanced Raman spectroscopy [41], stimulated Raman [42,43], and upconversion [44].
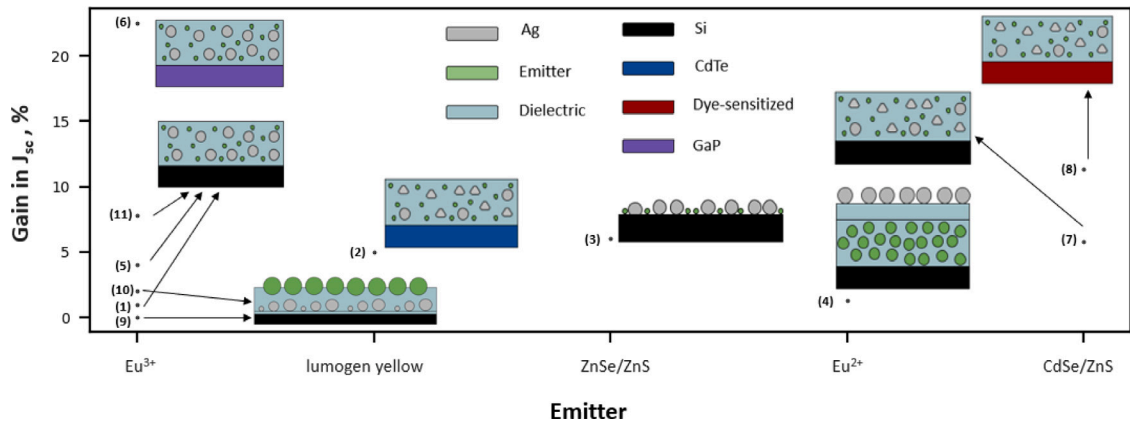
Table 1
Summary of experimentally demonstrated plasmon-enhanced DS ($p = 1$) and DC ($p > 1$) via plasmonic NPs.

Plasmonic NPs	Size, nm	Luminescence					Enhancement	Ref.
		host:emitter	p	λ_{exc}, nm	λ_{ems}, nm			
Ag	15	borate glass:Er^{3+}/Yb^{3+}	1	365	470, 570		–	[83]
	25–35	borate glass:Eu^{3+}	1	365	625		–	[84]
	465	$NaYF_4$:Yb^{3+},Er^{3+},Ce^{3+}	1	980	1525		25	[51]
	4–16	zinc-boro-tellurite glass:Er^{3+}	1	476	536, 550, 632		3.2, 4.1, 3.8	[64]
	50 × 90	β-$NaYF_4$:Pr^{3+} NPs	1	444	876, 1017		4	[54]
	50	β-$NaYF_4$:Tb^{3+} NPs	1	379	543		3.9	[37]
	50	YAG:Ce^{3+},Yb^{3+} films	1	455	540, 1030		3.5	[55]
	22	$GdVO_4$:Eu^{3+}	1	395	620		3.1	[65]
	30	CdZnSeS QDs	1	450	520		3	[66]
	5.6	Li_{20}-LaF_3-Al_2O_3-SiO_2 glass:Tb^{3+}	1	325	542		2.8	[67]
	3	$Ga_{10}Ge_{25}S_{65}$ glass:Er^{3+}	1	488	550		2	[68]
	–	Y_2O_3:Tb^{3+}	1	300	541		1.9	[69]
	20	YVO_4:Eu^{3+},Bi^{3+}	1	340	619		1.2	[70]
	100–150	β-$NaYF_4$:Tb^{3+},Yb^{3+} NPs	2	377	977		2.4	[52]
	20–150	KYF_4:Tb^{3+}, Yb^{3+}	2	374&485	975		1.9	[77]
	–	Y_2O_3:Yb^{3+}	2	300	978		1.5	[69]
	100	$NaBaPO_4$:Eu^{2+},Yb^{3+}	2	355	1004		1.2	[76]
	50	$NaYF_4$:Tb^{3+},Yb^{3+} NPs	2	467	978		1.1	[78]
	100	$NaBaPO_4$:Eu^{2+},Er^{3+}	3	352	1534		1.4	[81]
	90–100	$NaBaPO_4$:Er^{3+}	3&4	485&377	1534		1.8	[82]
	30–110	$NaBaPO_4$:Er^{3+} d/w Li^+	4	377	1534		2	[40]
Ag&Au	103 & 41×18[a]	Eu^{3+} film	1	360	582, 590, 612		19.8, 28.7, 53.5	[71]
	110×142[b]	InP@ZnS QDs	1	442	610		12.9	[38]
	90 & 120×20[c]	β-$NaYF_4$:Er^{3+} NPs	2	486	977		3.5	[79]
Au	400–467	$NaGdF_4$:Er^{3+},Yb^{3+},Nd^{3+},Ce^{3+} [d]	1	980	1527		6	[57]
	23×6	$LaPO_4$:Eu^{3+}	1	393	611		3	[39]
	3.4	sodium tellurite glass:Sm^{3+}	1	404	577, 614, 658, 718		1.9, 1.8, 2, 2.2	[72]
	10	CdSe/ZnS QDs	1	560	575		1.5	[73]
	10	YAG:Ce	1	375	550		1.2	[74]
	100–150	$NaYF_4$:Tb^{3+},Yb^{3+}	2	372	980		3.5	[80]
	90×15	β-$NaYF_4$:Tb^{3+}, Yb^{3+} NPs	2	377	977		3	[53]
Al	440(400)×180	CaF_2:Er^{3+},Yb^{3+}	1	980	1540		1.9	[56]
	50–70	quartz:DPA	1	260	410		1.3	[75]

[a] Ag NPs & Au NPs.
[b] Au@Ag core–shell NPs.
[c] Ag NPs & Au NPs.
[d] $NaGdF_4$:Yb,Er,Ce@$NaGdF_4$:Yb,Nd@$NaGdF_4$ core–shell–shell lanthanide NPs.
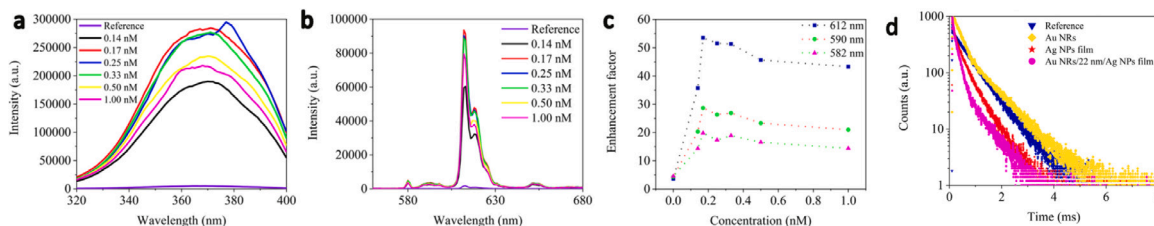
Fig. 5. Manifestation of plasmon-enhanced DS (example **11** from Fig. 4) in Eu^{3+}/Au NPs/PMMA/Ag NPs stack [71]. (a) Excitation spectra for 612 nm PL emission, (b) PL emission spectra under 360 nm excitation, and (c) PL enhancement factor at 582 nm, 590 nm, and 612 nm, all that for varying concentration of Au NPs at fixed concentration of Ag NPs. (d) Comparison of luminescence decay lifetime curves for emission at 612 nm for 3 different stacks: Eu^{3+}/Au NPs, Eu^{3+}/Ag NPs and Eu^{3+}/Au NPs/PMMA/Ag NPs.

- Time-resolved photolumienscence (PL) measurements demonstrated in Fig. 5(d) confirm that the relaxation time is decreased due to plasmon-enhanced decay rate of a fluorophore: from 662.25 μs for pure Eu^{3+} film to 310.3 μs for Eu^{3+}/Au NPs/PMMA/Ag NPs stack.

Fig. 6. Gain in short current density, J_{sc} (or short current I_{sc}) of PV modules due to plasmon-enhanced downconversion for different stack configurations and emitters used (see Table 2 for more details): **(1)** Eu^{3+} doped TeO_2–GeO_2–PbO glasses with silver nanoparticles on Si solar cell [97], **(2)** Poly(methyl methacrylate) polymer with lumogen yellow and Ag NPs deposited on top of CdTe mini-modules [98], **(3)** Si solar cell coated with ZnSe/ZnS QDs and Ag/ZnSe/ZnS QDs [99], **(4)** Ba_2SiO_4:7% Eu^{2+} nanophosphors, SiO_2 layer, and Ag NPs on Si solar cell [100], **(5)** Eu^{3+}-doped TeO_2-ZnO glass containing silver nanoparticles on Si solar cell [101], **(6)** Eu^{3+}-doped TeO_2-ZnO glass containing silver nanoparticles on GaP solar cell [101], **(7)** Poly(methyl methacrylate) polymer with core–shell quantum dots CdSe/ZnS and Ag NPs deposited on top of c-Si solar cell [102], **(8)** Poly(methyl methacrylate) polymer with core–shell quantum dots CdSe/ZnS and Ag NPs deposited on top of Dye-sensitized solar cell (DSSC) [102], **(9)** Si solar cell with Ag NPs embedded in a SiO_2 ARC mixed with Eu-doped phosphor particles [103], **(10)** Ag NPs with an SOG layer containing Eu-doped phosphors on Si solar cell [104], Metal-enhanced fluorescence layer of Ag-NPs/SOG:Eu-doped phosphors on Si solar cell [105], **(11)** Eu^{3+} doped tellurite glasses with Ag nanoparticles on Si-based solar cell [106].

Table 2
Summary of experimentally demonstrated plasmon-enhanced DS ($p = 1$ in all cases) for solar applications. Notice that for DSSC, DS layer deteriorates the performance [102], hence large gain due to plasmonics.

host:emitter	λ_{exc}, nm	λ_{ems}, nm	NP size	Bare cell		DS	DS+NP	NP gain	Ref.
				Cell	I_{sc} or J_{sc}				
SiO_2:Eu^{3+}	400	610	20	Si	26.29 mA/cm²	–	32.85	–	[103]
TeO_2-ZnO glass:Eu^{3+}	405 & 473	613	25	GaP	0.067 mA	0.071	0.087	22.5%	[101]
CdSe/ZnS QDs	300–500	500	45	DSSC	7.94 mA/cm²	7.35	8.18	11.3%	[102]
TeO_2-ZnO glass:Eu^{3+}	473	613	25	Si	0.279 mA	0.292	0.315	7.8%	[106]
ZnSe/ZnS QDs	300–400	420	20	Si	26.7 mA/cm²	29.4	31.2	6%	[99]
CdSe/ZnS QDs	300–500	500	45	Si	25.5 mA/cm²	25.99	27.5	5.8%	[102]
lumogen yellow	380	510	45	CdTe	11.5 mA/cm²	12.2	12.8	5%	[98]
TeO_2-ZnO glass:Eu^{3+}	405 & 473	613	25	Si	1.64 mA	1.72	1.79	4%	[101]
SOG:Eu^{3+}	370	514	18	Si	26.26 mA/cm²	32.24	32.91	2%	[104,105]
Ba_2SiO_4:Eu^{2+}	396	505	10–20	Si	41.18 mA/cm²	41.51	42.04	1.3%	[100]
TGP glass:Eu^{3+}	405	613	5	Si	8.27 mA	8.97	9.07	1%	[97]

4. Plasmon-enhanced downshifting and downconversion for solar energy conversion

The motivation for applying downshifting in solar energy harvesting lies in a fact that UV part of solar irradiance (about 4% of total energy reaching earth) is not utilized by photovoltaic (PV) modules efficiently. This amount of energy may seem to be incremental, however even small gain in solar cell performance has significant implications for a large-scale solar power plants. Moreover, cutting down the UV illumination which reaches PV module is by itself an important feature since UV degradation is a critical issue in photovoltaics [107–109].

The first demonstration of using DC for improving solar energy harvesting traces back to 1979 [110], when a substantial increase in quantum efficiency of low-cost CdS and amorphous-Si cells has been demonstrated. Later on, this concept has been heavily elaborated theoretically. For example, Trupke et al. [111] demonstrated maximum achievable 30.9% to 39.63% improvement for conversion efficiency of a solar cell in a presence of DC layer exposed directly to nonconcentrated radiation under the assumption of radiative recombination only. However, a detailed numerical analysis by Richards [11] reported quite concerning conclusions claiming that there are limited options for the successful application of rare-earth luminescent DC to silicon PV devices. Nonetheless, in the following decades this problem has been extensively studied both from materials science and theoretical perspectives: a comprehensive summary of DS and DC materials suitable for solar applications is given in Refs. [112–115], while more detailed theoretical analysis of solar cells performance in the presence of DS and DC materials under different conditions (but without plasmonic NPs) has been presented in several works [12,116–118].

We recall that the sole purpose of DS/DC is to convert high energy photons from UV to one or more photons with lower energy in visible or near-infrared range. In this case, external quantum efficiency (EQE) of PV module will be changed compared to PV module in the absence of any DS/DC material. It may appear to be counter-intuitive, but in the presence of DS/DC layer, EQE will

be modified in the wavelength range corresponding to the *absorption* spectra of DS/DC materials, *not to the emission* spectra. Simple yet insightful model describing a modification of EQE in the presence of DC/DS layers has been developed by Rothemund [116]. Considering several further elaborations of this formalism [117,118], it can be summarized as follows:

$$\mathrm{EQE}_{\mathrm{DS/DC}}(\lambda) = T_{\mathrm{PV}}(\lambda) \times \mathrm{IQE}(\lambda) +$$
$$+ A_{\mathrm{DS/DC}}(\lambda) \times \frac{\int T_{\mathrm{DS/DC \to PV}}(\lambda_{\mathrm{ems}}) \times \mathrm{IQE}(\lambda_{\mathrm{ems}}) \times \mathrm{QY}(\lambda, \lambda_{\mathrm{ems}}) \times \mathrm{PL}(\lambda, \lambda_{\mathrm{ems}}) \, \mathrm{d}\lambda_{\mathrm{ems}}}{\int \mathrm{PL}(\lambda, \lambda_{\mathrm{ems}}) \, \mathrm{d}\lambda_{\mathrm{ems}}} . \tag{4}$$

The first term in Eq. (4) corresponds to EQE calculated for PV module in presence of DS/DC material, assuming no emission due to DS/DC, i.e. this term explains how DS/DC material modifies the EQE just by the fact that it absorbs light:

- $T_{\mathrm{PV}}(\lambda)$ is the fraction of incident light transmitted directly to the PV layer;
- $\mathrm{IQE}(\lambda)$ is the internal quantum efficiency, which describes the inherent capability of the PV layer to convert absorbed light to electricity. The critical difference between EQE and IQE is that EQE takes as an input the *total* amount of photons incident to PV cell, while IQE takes as an input only photons which *reach* PV module, hence terms "external" and "internal". Obviously, $\mathrm{EQE}(\lambda) \leq \mathrm{IQE}(\lambda)$ at any given wavelength λ.

The second term in Eq. (4) describes a modification of EQE due to DS/DC emission:

- $A_{\mathrm{DS/DC}}(\lambda)$ is the fraction of light absorbed by DS/DC material. The largest possible absorption within UV together with the highest transparency in visible and/or infrared wavelength range are recommended for better utilization of DS/DC process;
- $T_{\mathrm{DS/DC \to PV}}(\lambda_{\mathrm{ems}})$ is the fraction of light emitted from DS/DC layer which reaches PV layer. It is critical to design the stack in such a way that the emitted light will not be trapped inside the DS/DC layer or leak into the air. Ideally, most of the light should reach PV layer. Recent work [117] shows that the amount of emitted light reaching PV layer dramatically changes from 10%–25% to 79%–90% by just changing the location of DS/DC layer within the stack;
- $\mathrm{PL}(\lambda, \lambda_{\mathrm{ems}})$ is photoluminescence spectra of the emitter;
- $\mathrm{QY}(\lambda, \lambda_{\mathrm{ems}})$ is the quantum yield of the emitter.

It is clear from Eq. (4) that PV modules with inherently low IQE in UV range are way much easier to boost via DC rather than modules with relatively high IQE in UV [119]. All that comes down to numerous issues and inconsistencies for correctly estimating boost in PV performance in the presence of luminescent layers with only recently established standards for characterization and reporting protocols [120].

Plasmonics has been widely studied and used for PV applications, numerous comprehensive reviews [28,121–124] summarize huge variety of possible scenarios, however, without a detailed discussion on downshifting and downconversion. The only available summary [125] of plasmon-enhanced DS in conjunction with PV devices presents a general discussion of this concept without providing references to any experimental examples. Analysis presented in Ref. [126] highlights the idea that incorporation of plasmonic NPs inevitably changes the entire optical response of the PV module, thus proper re-arrangement of the stack is required. In other words, the stack optimized without considering presence of plasmonic NPs will likely perform differently once plasmonic NPs are embedded in the system. Eq. (4) can be used to understand the impact of plasmonic NPs on PV performance:

- At the *micro scale*, considering the impact of any given single NP, the photoluminescence $\mathrm{PL}(\lambda, \lambda_{\mathrm{ems}})$ entering Eq. (4) will be enhanced by the factor of F according to Eq. (3);
- Once NPs are incorporated inside the emitting material, its refractive index becomes different from that of "pure" emitting material, even for relatively low concentration of plasmonic NPs. An extensive literature summarizes various strategies for taking this effect into account, depending on sizes, shapes and arrangements of NPs [127–129]. Once refractive index of the emitting layer is modified, it changes the way how light propagates through the stack and the way how light is emitted from the DS layer at the *macro scale*, that is $T_{\mathrm{PV}}(\lambda)$, $A_{\mathrm{DC}}(\lambda)$, and $T_{\mathrm{DC \to PV}}(\lambda_{\mathrm{ems}})$ entering Eq. (4) will be different in the presence of plasmonic NPs.

Recent comprehensive work [130] appears to be the only work attempting to incorporate the above optical effects into a single model capable of predicting and optimizing performance of PV modules in the presence of plasmonic NPs. The approach involves utilization of different techniques such as finite-difference time-domain method, Monte-Carlo simulations, ray tracing algorithms for finding size, shape and concentration of plasmonic NPs as well as luminescent species and host material for optimal performance of PV modules. Experimental efforts summarized in Table 2 and Fig. 6 are typically limited to a particular stack with a narrow range of variability of stack parameters. Nonetheless, an improvement in performance of various PV modules is observed with up to 22.5% boost in short current by just incorporating plasmonic NPs into the DS layer [101].

Fig. 7 demonstrates a detailed view on how EQE of solar modules and generated current are modified in the presence of "bare" DS layer and DS layer with plasmonic NPs embedded in it. EQE gains boost in UV range corresponding to the absorption spectra of DS materials involved, which is in agreement with Eq. (4). Further, the current density is also increased. Indeed, according to the definition of short current density,

$$J_{\mathrm{sc}} = \frac{q}{hc} \int_{\lambda} E(\lambda) \times \mathrm{EQE}(\lambda) \mathrm{d}\lambda , \tag{5}$$

one should expect to observe larger J_{sc} for boosted EQE. Here q is the electron charge, h is the Plank's constant, c is the speed of light in vacuum, $E(\lambda)$ is the source spectrum (i.e. the spectral irradiance incident on the solar module).
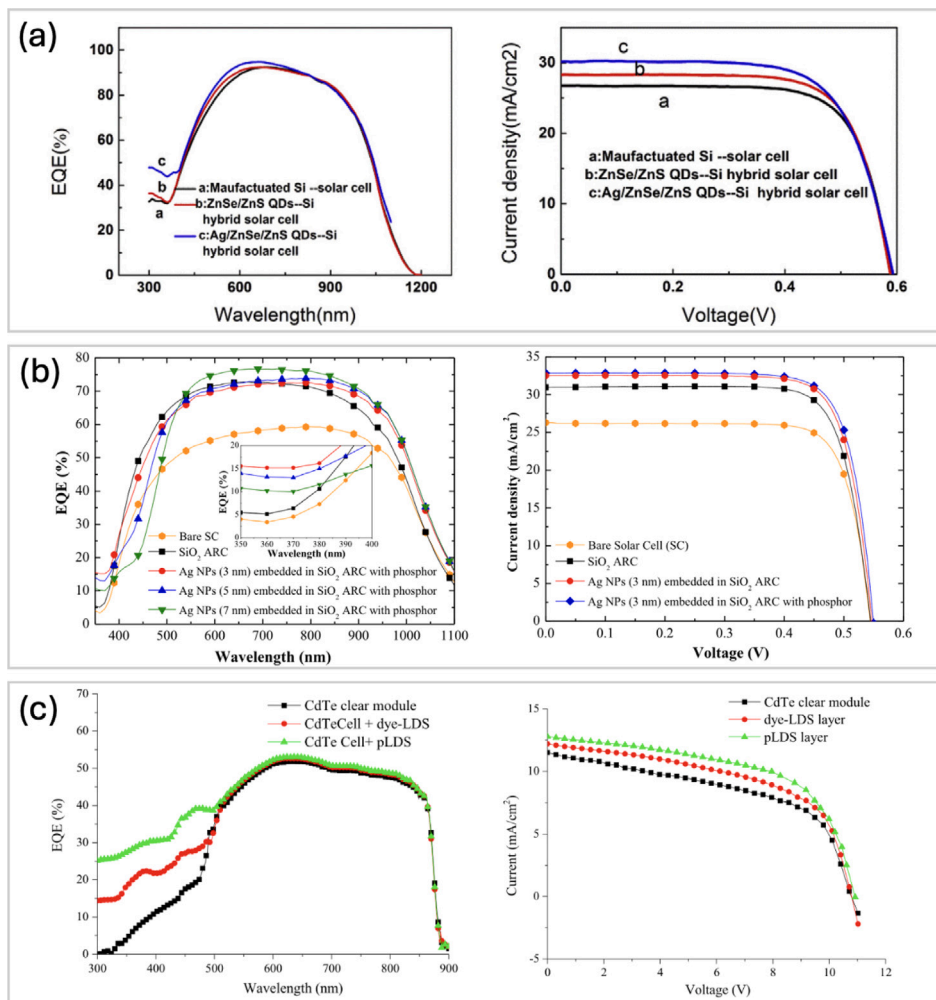
Fig. 7. EQE (left) and current–voltage characteristics (right) experimentally measured for different combinations of solar cells and DS materials, all that enhanced by Ag NPs (see configurations **(3)**, **(9)** and **(2)** from Fig. 6, respectively): (a) ZnSe/ZnS QDs with Si cell [99], (b) $SiO_2:Eu^{3+}$ with Si cell [103], (c) lumogen yellow with CdTe mini module [98]. Notice consistent increase of EQE in UV wavelength range (left) and improvement in current density (right) due to DS only and due to plasmon-enhanced DS in the presence of plasmonic NPs. For further details on experiments the reader is referred to original articles.

Besides the very boost of the performance of solar cells due to the DS phenomenon, a supplementary improvement of UV stability can be also harnessed with plasmonic NPs [70]. Nonetheless, the research on plasmon-enhanced DS with applications in solar industry appears to be in the early stage: only about a dozen of works with solid demonstration of boosting the performance are available, while proper optimization studies are apparently missing. Moreover, to the best of our knowledge, plasmon-enhanced DC for solar energy conversion has not been reported yet.

5. Conclusion and outlook

In this review, we have discussed fundamentals of plasmon-enhanced downshifting and downconversion, summarized the most representative experimental observations of this effect, and discussed implications to solar energy harvesting. To date, there is rich experimental evidence of plasmon-enhanced downshifting and downconversion, predominantly using Ag nanoparticles, with a few cases employing Au, and even fewer utilizing Al. The largest plasmon-enhanced downshifting reported so far is 53.5 for a combination of Ag and Au nanoparticles [71]. Numerical modeling and proper theoretical considerations with a search of optimal designs are clearly missing in the literature except several works reported detailed theoretical and experimental investigation of plasmon-enhanced downshifting [51] and its implications to solar cells [130]. Plasmonic enhancement has been studied for downconversion in white organic light emitting diodes [131] and bioimaging [51,57], but it appears that these are only few examples of combining plasmonic nanoparticles with downshifting or downconverting emitters in applications other than solar energy harvesting. The latter has been explored experimentally in a larger number of works summarized in Section 4.

That said, there is a plenty of room for further exploration of plasmon enhanced downshifting and downconversion, including but not limiting to the following:

- *Theoretical* and *numerical* analysis of plasmon-enhanced downshifting and downconversion beyond calculating electric fields. As demonstrated in Section 2 and in Ref. [51], plasmon-enhanced downshifting and downconversion processes are quite involved and require delicate balance between enhancement due to local electric field and quenching due to non-radiative decay rates.

- *Ordered arrays* of plasmonic nanoparticles for enhancing downshifting and downconversion are largely unexplored except few works [54,56,57]. We anticipate a great potential of harnessing structural resonances, such as collective lattice resonances [132,133] for enhancing downshifting and downconversion processes, which is already shown to be exceptionally efficient for fluorescence enhancement [134] and lasing [135–137].

Last but not the least, lossless *all-dielectric* nanoparticles [138] can serve as an attractive alternative for plasmonic nanoparticles to enhance downshifting and downconversion. Recent progress revealed successful utilization of all-dielectric nanoparticles for fluorescence [139–143] and upconversion [144,145] enhancement.

6. List of abbreviations

DC – downconversion
DPA – 9,10-Diphenylanthracene
DS – downshifting
DSSC – dye-sensitized solar cell
EQE – external quantum efficiency
IQE - internal quantum efficiency
NP – nanoparticle
PL – photoluminescence
PLMA – poly(lauryl methacrylate)
PMMA – poly(methyl methacrylate)
PS – polystyrene
PV – photovoltaic
PVA – polyvinyl alcohol
QD – quantum dot
TGP – TeO_2-GeO_2-PbO
UV – ultraviolet

Declaration of competing interest

The authors declare that they have no known competing financial interests or personal relationships that could have appeared to influence the work reported in this paper.

References

[1] D.L. Dexter, Possibility of luminescent quantum yields greater than unity, Phys. Rev. 108 (3) (1957) 630–633, http://dx.doi.org/10.1103/PhysRev.108.630.

[2] F. Auzel, Compteur quantique par transfert d'energie entre deux ions de terres rares dans un tungstate mixte et dans un verre, C. R. Acad. Sci. Paris 262 (1966) 1016–1019.

[3] J. Sommerdijk, A. Bril, A. De Jager, Two photon luminescence with ultraviolet excitation of trivalent praseodymium, J. Lumin. 8 (4) (1974) 341–343, http://dx.doi.org/10.1016/0022-2313(74)90006-4.

[4] J. Sommerdijk, A. Bril, A. De Jager, Luminescence of Pr^{3+}-activated fluorides, J. Lumin. 9 (4) (1974) 288–296, http://dx.doi.org/10.1016/0022-2313(74)90041-6.

[5] W. Piper, J. DeLuca, F. Ham, Cascade fluorescent decay in Pr^{3+}-doped fluorides: Achievement of a quantum yield greater than unity for emission of visible light, J. Lumin. 8 (4) (1974) 344–348, http://dx.doi.org/10.1016/0022-2313(74)90007-6.

[6] R.T. Wegh, H. Donker, K.D. Oskam, A. Meijerink, Visible quantum cutting in $LiGdF_4$:Eu^{3+} through downconversion, Science 283 (5402) (1999) 663–666, http://dx.doi.org/10.1126/science.283.5402.663.

[7] R. Wegh, H. Donker, E. Van Loef, K. Oskam, A. Meijerink, Quantum cutting through downconversion in rare-earth compounds, J. Lumin. 87–89 (2000) 1017–1019, http://dx.doi.org/10.1016/S0022-2313(99)00514-1.

[8] K. Oskam, R. Wegh, H. Donker, E. Van Loef, A. Meijerink, Downconversion: a new route to visible quantum cutting, J. Alloys Compd. 300–301 (2000) 421–425, http://dx.doi.org/10.1016/S0925-8388(99)00755-0.

[9] Y. Zhong, H. Dai, A mini-review on rare-earth down-conversion nanoparticles for NIR-II imaging of biological systems, Nano Res. 13 (5) (2020) 1281–1294, http://dx.doi.org/10.1007/s12274-020-2721-0.

[10] C.H. Kang, Y. Wang, O. Alkhazragi, H. Lu, T.K. Ng, B.S. Ooi, Down-converting luminescent optoelectronics and their applications, APL Photon. 8 (2) (2023) 020903, http://dx.doi.org/10.1063/5.0127552.

[11] B. Richards, Luminescent layers for enhanced silicon solar cell performance: Down-conversion, Sol. Energy Mater. Sol. Cells 90 (9) (2006) 1189–1207, http://dx.doi.org/10.1016/j.solmat.2005.07.001.

[12] A.M. Gabr, J.F. Wheeldon, R.M. Beal, A. Walker, J. Sacks, R.M. Savidge, T.J. Hall, R.N. Kleiman, K. Hinzer, Modeling down-conversion and downshifting for photovoltaic applications, in: 2012 38th IEEE Photovoltaic Specialists Conference, IEEE, Austin, TX, USA, 2012, pp. 000048–000052, http://dx.doi.org/10.1109/PVSC.2012.6317566.

[13] A. Mayavan, Comprehensive review on downconversion/downshifting silicate-based phosphors for solar cell applications, ACS Omega 9 (15) (2024) 16880–16892, http://dx.doi.org/10.1021/acsomega.3c08806.

[14] W. Van, A. Meijerink, R. Schropp, Solar spectrum conversion for photovoltaics using nanoparticles, in: V. Fthenakis (Ed.), Third Generation Photovoltaics, InTech, 2012, URL http://www.intechopen.com/books/third-generation-photovoltaics/solar-spectrum-conversion-for-photovoltaics-using-nanoparticles.

[15] Y. Yu, L. Lan, H. Cai, Integrating down-shifting and down-conversion into metal–organic frameworks to enhance the spectral conversion for solar cells, J. Phys. Chem. C 122 (1) (2018) 96–104, http://dx.doi.org/10.1021/acs.jpcc.7b09184.

[16] Z. Artvin, M. Gunay, A. Bek, M.E. Tasgin, Fano-control of down-conversion in a nonlinear crystal via plasmonic–quantum emitter hybrid structures, J. Opt. Soc. Am. B 37 (12) (2020) 3769–3776, http://dx.doi.org/10.1364/JOSAB.405637.

[17] Z. Wang, A. Meijerink, Dye-sensitized downconversion, J. Phys. Chem. Lett. 9 (7) (2018) 1522–1526, http://dx.doi.org/10.1021/acs.jpclett.8b00516.

[18] J. Hong, L. Lin, X. Li, J. Xie, Q. Qin, Z. Zheng, Enhancement of near-infrared quantum-cutting luminescence in $NaBaPO_4$:Er^{3+} phosphors by Bi^{3+}, Opt. Mater. 98 (2019) 109471, http://dx.doi.org/10.1016/j.optmat.2019.109471.

[19] K.M. McPeak, S.V. Jayanti, S.J.P. Kress, S. Meyer, S. Iotti, A. Rossinelli, D.J. Norris, Plasmonic films can easily be better: Rules and recipes, ACS Photon 2 (3) (2015) 326–333, http://dx.doi.org/10.1021/ph5004237.

[20] P.B. Johnson, R.W. Christy, Optical constants of the noble metals, Phys. Rev. B 6 (12) (1972) 4370–4379, http://dx.doi.org/10.1103/PhysRevB.6.4370.

[21] I.L. Rasskazov, P.S. Carney, A. Moroz, STRATIFY: a comprehensive and versatile MATLAB code for a multilayered sphere, OSA Contin. 3 (8) (2020) 2290–2309, http://dx.doi.org/10.1364/OSAC.399979.

[22] E. Ozbay, Plasmonics: Merging photonics and electronics at nanoscale dimensions, Science 311 (5758) (2006) 189–193, http://dx.doi.org/10.1126/science.1114849.

[23] J.A. Schuller, E.S. Barnard, W. Cai, Y.C. Jun, J.S. White, M.L. Brongersma, Plasmonics for extreme light concentration and manipulation, Nature Mater. 9 (3) (2010) 193–204, http://dx.doi.org/10.1038/nmat2630.

[24] D.K. Gramotnev, S.I. Bozhevolnyi, Plasmonics beyond the diffraction limit, Nat. Photonics 4 (2) (2010) 83–91, http://dx.doi.org/10.1038/nphoton.2009.282.

[25] M.I. Stockman, Nanoplasmonics: past, present, and glimpse into future, Opt. Express 19 (22) (2011) 22029–22106, http://dx.doi.org/10.1364/OE.19.022029.

[26] A.N. Grigorenko, M. Polini, K.S. Novoselov, Graphene plasmonics, Nat. Photonics 6 (11) (2012) 749–758, http://dx.doi.org/10.1038/nphoton.2012.262.

[27] E. Ringe, B. Sharma, A.-I. Henry, L.D. Marks, R.P. Van Duyne, Single nanoparticle plasmonics, Phys. Chem. Chem. Phys. 15 (12) (2013) 4110–4129, http://dx.doi.org/10.1039/c3cp44574g.

[28] H.A. Atwater, A. Polman, Plasmonics for improved photovoltaic devices, Nature Mater. 9 (3) (2010) 205–213, http://dx.doi.org/10.1038/nmat2629.

[29] M. Kauranen, A.V. Zayats, Nonlinear plasmonics, Nat. Photonics 6 (11) (2012) 737–748, http://dx.doi.org/10.1038/nphoton.2012.244.

[30] S.I. Azzam, A.V. Kildishev, R.-M. Ma, C.-Z. Ning, R. Oulton, V.M. Shalaev, M.I. Stockman, J.-L. Xu, X. Zhang, Ten years of spasers and plasmonic nanolasers, Light: Sci. Appl. 9 (1) (2020) 90, http://dx.doi.org/10.1038/s41377-020-0319-7.

[31] L.K. Sørensen, V. Gerasimov, S.V. Karpov, H. Ågren, Development of discrete interaction models for ultra-fine nanoparticle plasmonics, Phys. Chem. Chem. Phys. 26 (2024) 24209–24245, http://dx.doi.org/10.1039/D4CP00778F.

[32] G. Mie, Beiträge zur Optik trüber Medien, speziell kolloidaler Metallösungen, Ann. Phys., Lpz. 330 (3) (1908) 377–445, http://dx.doi.org/10.1002/andp.19083300302.

[33] C.F. Bohren, D.R. Huffman, Absorption and Scattering of Light By Small Particles, Wiley-VCH Verlag GmbH, Weinheim, Germany, 1998, URL http://doi.wiley.com/10.1002/9783527618156.

[34] P. Anger, P. Bharadwaj, L. Novotny, Enhancement and quenching of single-molecule fluorescence, Phys. Rev. Lett. 96 (11) (2006) 113002, http://dx.doi.org/10.1103/PhysRevLett.96.113002.

[35] P. Bharadwaj, L. Novotny, Spectral dependence of single molecule fluorescence enhancement, Opt. Express 15 (21) (2007) 14266–14274, http://dx.doi.org/10.1364/oe.15.014266.

[36] I.L. Rasskazov, A. Moroz, Is there a proper figure of merit for a plasmonic structure involved in metal-enhanced fluorescence? Plasmonics 17 (3) (2022) 1091–1094, http://dx.doi.org/10.1007/s11468-022-01601-2.

[37] L. Lin, Z. Yu, Z. Wang, B. Zheng, Z. Feng, Z. Zheng, Plasmon-enhanced luminescence of $Ag@SiO_2/\beta$-$NaYF_4$:Tb^{3+} nanocomposites via absorption & emission matching, Mater. Chem. Phys. 220 (2018) 278–285, http://dx.doi.org/10.1016/j.matchemphys.2018.08.076.

[38] K.-S. Kim, M. Zakia, J. Yoon, S.I. Yoo, Metal-enhanced fluorescence in polymer composite films with $Au@Ag@SiO_2$ nanoparticles and $InP@ZnS$ quantum dots, RSC Adv. 9 (1) (2019) 224–233, http://dx.doi.org/10.1039/C8RA08802K.

[39] S. Kuzman, J. Periša, V. Đorđević, I. Zeković, I. Vukoje, Z. Antić, M.D. Dramićanin, Surface plasmon enhancement of Eu^{3+} emission intensity in $LaPO_4$/Ag nanoparticles, Materials 13 (14) (2020) 3071, http://dx.doi.org/10.3390/ma13143071.

[40] J. Hong, B. Zheng, Q. Cheng, J. Wang, Y. Liu, R. Lin, K. Li, L. Huang, J. Wang, L. Lin, Z. Zheng, Simultaneous enhancement of quantum cutting luminescence in Er-doped $NaBaPO_4$ phosphors by crystal field control and plasmonic modulation, Ceram. Int. 48 (20) (2022) 29730–29741, http://dx.doi.org/10.1016/j.ceramint.2022.06.233.

[41] T. van Dijk, S.T. Sivapalan, B.M. DeVetter, T.K. Yang, M.V. Schulmerich, C.J. Murphy, R. Bhargava, P.S. Carney, Competition between extinction and enhancement in surface-enhanced Raman spectroscopy, J. Phys. Chem. Lett. 4 (7) (2013) 1193–1196, http://dx.doi.org/10.1366/12-06847.

[42] B.X.K. Chng, T. van Dijk, R. Bhargava, P.S. Carney, Enhancement and extinction effects in surface-enhanced stimulated Raman spectroscopy, Phys. Chem. Chem. Phys. 17 (33) (2015) 21348–21355, http://dx.doi.org/10.1039/C4CP05089D.

[43] N.L. Gruenke, M.O. McAnally, G.C. Schatz, R.P. Van Duyne, Balancing the effects of extinction and enhancement for optimal signal in surface-enhanced femtosecond stimulated Raman spectroscopy, J. Phys. Chem. C 120 (51) (2016) 29449–29454, http://dx.doi.org/10.1021/acs.jpcc.6b10727.

[44] I.L. Rasskazov, L. Wang, C.J. Murphy, R. Bhargava, P.S. Carney, Plasmon-enhanced upconversion: engineering enhancement and quenching at nano and macro scales, Opt. Mater. Express 8 (12) (2018) 3787–3804, http://dx.doi.org/10.1364/OME.8.003787.

[45] M.J.A. de Dood, L.H. Slooff, A. Polman, A. Moroz, A. van Blaaderen, Modified spontaneous emission in erbium-doped SiO_2 spherical colloids, Appl. Phys. Lett. 79 (22) (2001) 3585–3587, http://dx.doi.org/10.1063/1.1419033.

[46] G.S. Ofelt, Intensities of crystal spectra of rare-earth ions, J. Chem. Phys. 37 (3) (1962) 511–520, http://dx.doi.org/10.1063/1.1701366.

[47] B.M. Walsh, N.P. Barnes, B. Di Bartolo, Branching ratios, cross sections, and radiative lifetimes of rare earth ions in solids: Application to Tm^{3+} and Ho^{3+} ions in $LiYF_4$, J. Appl. Phys. 83 (5) (1998) 2772–2787, http://dx.doi.org/10.1063/1.367037.

[48] R. Nagaishi, T. Kimura, S.P. Sinha, Luminescence properties of lanthanide(III) ions in concentrated carbonate solution, Mol. Phys. 101 (7) (2003) 1007–1014, http://dx.doi.org/10.1080/0026897021000046861.

[49] N. Luewarasirikul, J. Kaewkhao, Spectroscopic properties and Judd–Ofelt analysis of Eu^{3+} doped Ba-Na-B glasses for photonic applications, J. Conf. Ser. 1819 (1) (2021) 012072, http://dx.doi.org/10.1088/1742-6596/1819/1/012072.

[50] A.D. Utyushev, R. Gaponenko, S. Sun, A.A. Shcherbakov, A. Moroz, I.L. Rasskazov, Generation of nearly pure and highly directional magnetic light in fluorescence of rare-earth ions, Phys. Rev. B 109 (4) (2024) 045413, http://dx.doi.org/10.1103/PhysRevB.109.045413.

[51] J. Xu, M. Fu, Y. Lu, A. Centeno, J. Xu, X. Xiao, Q. Zhang, K. Evers, Y. Xu, R. Lim, C. Liu, S.A. Maier, R. Oulton, M.P. Ryan, F. Xie, Remarkable plasmonic enhanced luminescence of Ce^{3+} doped lanthanide downconversion nanoparticles in NIR-II window by silver hole-cap nanoarrays, Adv. Opt. Mater. (2024) 2400660, http://dx.doi.org/10.1002/adom.202400660.

[52] B. Zheng, L. Lin, Z. Feng, Z. Yu, Z. Wang, S. Xu, Z. Zheng, Plasmon enhanced near-infrared quantum cutting and simulation analysis of β-NaYF$_4$:Tb^{3+}, Yb^{3+} doped with Ag nanoparticles, Opt. Mater. Express 7 (1) (2017) 224–230, http://dx.doi.org/10.1364/OME.7.000224.

[53] B. Zheng, L. Lin, Z. Feng, L. Huang, L. Zhuang, Z. Wang, Z. Zheng, Enhanced quantum cutting luminescence by Au nanorods through improving radiative transition rate, Opt. Commun. 402 (2017) 336–339, http://dx.doi.org/10.1016/j.optcom.2017.06.041.

[54] B. Zheng, J. Wang, L. Lin, J. Hong, L. Huang, Y. Li, Z. Feng, Z. Wang, Z. Zheng, Plasmon enhanced near-infrared downconversion luminescence of β-NaYF$_4$:Pr^{3+} nanoparticles by high-ordered Ag nanopillar arrays with tunable nanogaps, Opt. Mater. Express 8 (11) (2018) 3401–3409, http://dx.doi.org/10.1364/ome.8.003401.

[55] M. Kushlyk, V. Tsiumra, Y. Zhydachevskyy, V. Haiduchok, I. Syvorotka, D. Sugak, A. Suchocki, Enhancement of the YAG: Ce, Yb down-conversion emission by plasmon resonance in Ag nanoparticles, J. Alloys Compd. 804 (2019) 202–212, http://dx.doi.org/10.1016/j.jallcom.2019.06.382.

[56] Y. Gao, S. Murai, S. Tamura, K. Tomita, K. Tanaka, Enhancement of up- and downconversion photoluminescence from Yb^{3+}, Er^{3+} co-doped CaF$_2$ nanoparticles deposited on two-dimensional plasmonic arrays, in: S. Kawata, M. Qiu, H. Xu (Eds.), Plasmonics IV, SPIE, 2019, p. 19, http://dx.doi.org/10.1117/12.2538731.

[57] J. Xu, M. Fu, C. Ji, A. Centeno, D.K. Kim, K. Evers, S.E.M. Heutz, R. Oulton, M.P. Ryan, F. Xie, Plasmonic-enhanced NIR-II downconversion fluorescence beyond 1500 nm from core–shell–shell lanthanide nanoparticles, Adv. Opt. Mater. 11 (19) (2023) 2300477, http://dx.doi.org/10.1002/adom.202300477.

[58] C. Geddes, J. Lakowicz, Metal-enhanced fluorescence, J. Fluorescence 12 (2) (2002) 121–129, http://dx.doi.org/10.1023/A:1016875709579.

[59] J.R. Lakowicz, K. Ray, M. Chowdhury, H. Szmacinski, Y. Fu, J. Zhang, K. Nowaczyk, Plasmon-controlled fluorescence: a new paradigm in fluorescence spectroscopy, Analyst 133 (10) (2008) 1308–1346, http://dx.doi.org/10.1039/b802918k.

[60] D.M. Wu, A. García-Etxarri, A. Salleo, J.A. Dionne, Plasmon-enhanced upconversion, J. Phys. Chem. Lett. 5 (22) (2014) 4020–4031, http://dx.doi.org/10.1021/jz5019042.

[61] W. Park, D. Lu, S. Ahn, Plasmon enhancement of luminescence upconversion, Chem. Soc. Rev. 44 (10) (2015) 2940–2962, http://dx.doi.org/10.1039/C5CS00050E.

[62] W. Xu, X. Chen, H. Song, Upconversion manipulation by local electromagnetic field, Nano Today 17 (2017) 54–78, http://dx.doi.org/10.1016/j.nantod.2017.10.011.

[63] J. Dong, W. Gao, Q. Han, Y. Wang, J. Qi, X. Yan, M. Sun, Plasmon-enhanced upconversion photoluminescence: Mechanism and application, Rev. Phys. 4 (2019) 100026, http://dx.doi.org/10.1016/j.revip.2018.100026.

[64] Z.A. Said Mahraz, M. Sahar, S. Ghoshal, Enhanced luminescence from silver nanoparticles integrated Er^{3+}-doped boro-tellurite glasses: Impact of annealing temperature, J. Alloys Compd. 649 (2015) 1102–1109, http://dx.doi.org/10.1016/j.jallcom.2015.07.232.

[65] S. Bishnoi, S. Chawla, Enhancement of GdVO$_4$:Eu^{3+} red fluorescence through plasmonic effect of silver nanoprisms on Si solar cell surface, J. Appl. Res. Technol. 15 (2) (2017) 102–109, http://dx.doi.org/10.1016/j.jart.2017.01.007.

[66] H. Kim, N. Heo, B. Kim, S. Yoon, Y. Jae Cho, J. Choi, K.-T. Lee, S. Park, D. Bin Kim, Y. Kim, T. Kwak, J. Lee, D.-H. Ko, Synthetic hybrid particles to improve the down-conversion efficiency of quantum dots via simultaneously induced scattering and plasmonic effects, Chem. Eng. J. 450 (2022) 138270, http://dx.doi.org/10.1016/j.cej.2022.138270.

[67] P. Piasecki, Formation of Ag nanoparticles and enhancement of Tb^{3+} luminescence in Tb and Ag co-doped lithium-lanthanum-aluminosilicate glass, J. Nanophoton. 4 (1) (2010) 043522, http://dx.doi.org/10.1117/1.3528943.

[68] Z. Pan, A. Ueda, R. Aga, A. Burger, R. Mu, S. Morgan, Spectroscopic studies of Er^{3+} doped Ge-Ga-S glass containing silver nanoparticles, J. Non-Cryst. Solids 356 (23–24) (2010) 1097–1101, http://dx.doi.org/10.1016/j.jnoncrysol.2010.04.014.

[69] Q. Sun, S. Zhan, E. Liu, H. Miao, Y. Hao, G. Zhang, D. Zhang, J. Fan, X. Hu, The preparation and study of fluorescence properties of Y$_2$O$_3$:Tb^{3+}, Yb^{3+} doped with silver nanoparticles, Ceram. Int. 41 (10) (2015) 12644–12650, http://dx.doi.org/10.1016/j.ceramint.2015.06.095.

[70] C.-K. Wu, S. Zou, C.-W. Peng, S.-W. Gu, M.-F. Ni, Y.-L. Zeng, H. Sun, X.-H. Zhang, X.-D. Su, Improving the UV-light stability of silicon heterojunction solar cells through plasmon-enhanced luminescence downshifting of YVO$_4$:Eu^{3+}, Bi^{3+} nanophosphors decorated with Ag nanoparticles, J. Energy Chem. 81 (2023) 212–220, http://dx.doi.org/10.1016/j.jechem.2023.01.050.

[71] J. Liu, X. Zhao, X. Liu, D. Zhang, Q. Wang, L. Zhang, S. Li, Q. Shi, C. Liu, B. Zhang, W. Wang, Q. Wang, Enhanced luminescence of Eu-doped films based on gap coupled plasmons, J. Alloys Compd. 907 (2022) 164451, http://dx.doi.org/10.1016/j.jallcom.2022.164451.

[72] S.Q. Mawlud, M.M. Ameen, M.R. Sahar, K.F. Ahmed, Plasmon-enhanced luminescence of samarium doped sodium tellurite glasses embedded with gold nanoparticles: Judd–Ofelt parameter, J. Lumin. 190 (2017) 468–475, http://dx.doi.org/10.1016/j.jlumin.2017.06.004.

[73] S. Chandra, J. Doran, S. McCormack, M. Kennedy, A. Chatten, Enhanced quantum dot emission for luminescent solar concentrators using plasmonic interaction, Sol. Energy Mater. Sol. Cells 98 (2012) 385–390, http://dx.doi.org/10.1016/j.solmat.2011.11.030.

[74] V. Ţucureanu, D. Munteanu, Enhanced optical properties of YAG:Ce yellow phosphor by modification with gold nanoparticles, Ceram. Int. 45 (6) (2019) 7641–7648, http://dx.doi.org/10.1016/j.ceramint.2019.01.061.

[75] R. Mupparapu, K. Vynck, I. Malfanti, S. Vignolini, M. Burresi, P. Scudo, R. Fusco, D.S. Wiersma, Enhanced downconversion of UV light by resonant scattering of aluminum nanoparticles, Opt. Lett. 37 (3) (2012) 368–370, http://dx.doi.org/10.1364/OL.37.000368.

[76] L. Lin, J. Chen, Z. Wang, Z. Feng, F. Huang, B. Zheng, L. Huang, Z. Yu, Z. Zheng, Plasmon-enhanced broad-band quantum-cutting of NaBaPO$_4$:Eu^{2+}, Yb^{3+} phosphor decorated with Ag nano-particles, Mater. Res. Bull. 93 (2017) 35–41, http://dx.doi.org/10.1016/j.materresbull.2017.04.043.

[77] B. Zheng, S. Xu, L. Lin, Z. Wang, Z. Feng, Z. Zheng, Plasmon enhanced near-infrared quantum cutting of KYF$_4$:Tb^{3+}, Yb^{3+} doped with Ag nanoparticles, Opt. Lett. 40 (11) (2015) 2630–2633, http://dx.doi.org/10.1364/OL.40.002630.

[78] F. He, Q. Wang, Z. Song, Z. Wang, T. Xiao, Y. Fan, T. Wang, Enhancement of Tb–Yb quantum cutting luminescence with Ag nanostructures and photonic crystals, Opt. Mater. 109 (2020) 110421, http://dx.doi.org/10.1016/j.optmat.2020.110421.

[79] L. Huang, L. Lin, B. Zheng, H. Huang, Z. Feng, Z. Wang, X. Li, Z. Zheng, Simultaneous excitation and emission enhancement of near-infrared quantum cutting in β-NaYF$_4$:Er^{3+} nanoparticles by double plasmon modes of noble metals, Opt. Commun. 441 (2019) 170–175, http://dx.doi.org/10.1016/j.optcom.2019.02.048.

[80] L. Lin, Z. Yu, Z. Wang, Z. Feng, F. Huang, L. Huang, Q. Dai, F. Zhang, Z. Zheng, Plasmon-enhanced upconversion and quantum-cutting of water-soluble Au@SiO$_2$/NaYF$_4$:Tb^{3+}, Yb^{3+}@NaYF$_4$ nanocomposites, J. Lumin. 214 (2019) 116598, http://dx.doi.org/10.1016/j.jlumin.2019.116598.

[81] J. Hong, L. Lin, X. Li, Z. Feng, L. Huang, Q. Qin, Z. Zheng, Plasmon-enhanced broad-band quantum-cutting of NaBaPO$_4$:Eu^{2+}, Er^{3+} phosphors with silver nano-particles, J. Rare Earths 38 (11) (2020) 1151–1157, http://dx.doi.org/10.1016/j.jre.2019.12.002.

[82] J.-Q. Hong, B. Zheng, R.-L. Zeng, Y.-X. Xiu, R.-y. Zeng, K.-X. Lin, D.-Q. Chen, Multi-photon near-infrared quantum cutting enhancement by surface plasmon of Ag nanoparticles under multi-excitation, Chin. J. Lumin. 43 (7) (2022) 1052–1060, http://dx.doi.org/10.37188/CJL.20220138.

[83] C.-h. Bae, K.-S. Lim, Enhanced blue emission in Er^{3+}/Yb^{3+} doped glass-ceramics containing Ag nanoparticles and ZnO nanocrystals, Curr. Opt. Photon. 3 (2) (2019) 135–142, http://dx.doi.org/10.3807/COPP.2019.3.2.135.

[84] C.-h. Bae, K.-S. Lim, Enhanced visible emission in Eu^{3+} doped glass containing Ag-clusters, Ag nanoparticles, and ZnO nanocrystals, J. Alloys Compd. 793 (2019) 410–417, http://dx.doi.org/10.1016/j.jallcom.2019.04.122.

[85] M.W. Knight, N.S. King, L. Liu, H.O. Everitt, P. Nordlander, N.J. Halas, Aluminum for plasmonics, ACS Nano 8 (1) (2014) 834–840, http://dx.doi.org/10.1021/nn405495q.

[86] D. Gérard, S.K. Gray, Aluminium plasmonics, J. Phys. D: Appl. Phys. 48 (18) (2015) 184001, http://dx.doi.org/10.1088/0022-3727/48/18/184001.

[87] X. Zhu, G.M. Imran Hossain, M. George, A. Farhang, A. Cicek, A.A. Yanik, Beyond noble metals: High Q-factor aluminum nanoplasmonics, ACS Photon. 7 (2) (2020) 416–424, http://dx.doi.org/10.1021/acsphotonics.9b01368.

[88] P.-C. Chen, X. Liu, J.L. Hedrick, Z. Xie, S. Wang, Q.-Y. Lin, M.C. Hersam, V.P. Dravid, C.A. Mirkin, Polyelemental nanoparticle libraries, Science 352 (6293) (2016) 1565–1569, http://dx.doi.org/10.1126/science.aaf8402.

[89] G.D. Förster, M. Benoit, J. Lam, Alloy, Janus and core–shell nanoparticles: numerical modeling of their nucleation and growth in physical synthesis, Phys. Chem. Chem. Phys. 21 (41) (2019) 22774–22781, http://dx.doi.org/10.1039/C9CP04231H.

[90] D.M. Hofmann, D.H. Fairbrother, R.J. Hamers, C.J. Murphy, Two-phase synthesis of gold–copper bimetallic nanoparticles of tunable composition: Toward optimized catalytic CO_2 reduction, ACS Appl. Nano Mater. 2 (6) (2019) 3989–3998, http://dx.doi.org/10.1021/acsanm.9b00904.

[91] R. Borah, S.W. Verbruggen, Silver-gold bimetallic alloy versus core–shell nanoparticles: Implications for plasmonic enhancement and photothermal applications, J. Phys. Chem. C 124 (22) (2020) 12081–12094, http://dx.doi.org/10.1021/acs.jpcc.0c02630.

[92] A. Yasuhara, K. Kubo, S. Yanagimoto, T. Sannomiya, Thermodynamic tuning of Au–Ag–Cu nanoparticles with phase separation and ordered phase formation, J. Phys. Chem. C 124 (28) (2020) 15481–15488, http://dx.doi.org/10.1021/acs.jpcc.0c02834.

[93] G. González-Rubio, P. Díaz-Núñez, W. Albrecht, V. Manzaneda-González, L. Bañares, A. Rivera, L.M. Liz-Marzán, O. Peña-Rodríguez, S. Bals, A. Guerrero-Martínez, Controlled alloying of Au@Ag core–shell nanorods induced by femtosecond laser irradiation, Adv. Opt. Mater. 9 (10) (2021) 2002134, http://dx.doi.org/10.1002/adom.202002134.

[94] L.K. Sørensen, A.D. Utyushev, V.I. Zakomirnyi, H.Å. gren, Atomistic description of plasmonic generation in alloys and core shell nanoparticles, Phys. Chem. Chem. Phys. 23 (1) (2021) 173–185, http://dx.doi.org/10.1039/D0CP04854B.

[95] J.S. Biggins, S. Yazdi, E. Ringe, Magnesium nanoparticle plasmonics, Nano Lett. 18 (6) (2018) 3752–3758, http://dx.doi.org/10.1021/acs.nanolett.8b00955.

[96] E. Ringe, Shapes, plasmonic properties, and reactivity of magnesium nanoparticles, J. Phys. Chem. C 124 (29) (2020) 15665–15679, http://dx.doi.org/10.1021/acs.jpcc.0c03871.

[97] G. Mattos, C. Bordon, L. Gómez-Malagón, R. Gunji, L. Kassab, Performance improvement of Si solar cell via down-conversion and plasmonic processes using Eu^{3+} doped TeO_2-GeO_2-PbO glasses with silver nanoparticles as cover layer, J. Lumin. 238 (2021) 118271, http://dx.doi.org/10.1016/j.jlumin.2021.118271.

[98] H. Ahmed, S. McCormack, J. Doran, Plasmonic luminescent down shifting layers for the enhancement of CdTe mini-modules performance, Sol. Energy 141 (2017) 242–248, http://dx.doi.org/10.1016/j.solener.2016.11.036.

[99] N. Liu, H. Xue, Y. Ji, J. Wang, ZnSe/ZnS core–shell quantum dots incorporated with Ag nanoparticles as luminescent down-shifting layers to enhance the efficiency of Si solar cells, J. Alloys Compd. 747 (2018) 696–702, http://dx.doi.org/10.1016/j.jallcom.2018.03.060.

[100] J.-Y. Chen, C. Huang, W. Hung, K. Sun, T. Chen, Efficiency improvement of Si solar cells using metal-enhanced nanophosphor fluorescence, Sol. Energy Mater. Sol. Cells 120 (2014) 168–174, http://dx.doi.org/10.1016/j.solmat.2013.08.039.

[101] B.C. Lima, L.A. Gómez-Malagón, A.S.L. Gomes, J.A.M. Garcia, L.R.P. Kassab, Plasmon-assisted efficiency enhancement of Eu^{3+}-doped tellurite glass-covered solar cells, J. Electron. Mater. 46 (12) (2017) 6750–6755, http://dx.doi.org/10.1007/s11664-017-5744-x.

[102] H. Ahmed, J. Doran, S. McCormack, Increased short-circuit current density and external quantum efficiency of silicon and dye sensitised solar cells through plasmonic luminescent down-shifting layers, Sol. Energy 126 (2016) 146–155, http://dx.doi.org/10.1016/j.solener.2016.01.003.

[103] W.-J. Ho, S.-K. Feng, J.-J. Liu, Y.-C. Yang, C.-H. Ho, Improving photovoltaic performance of silicon solar cells using a combination of plasmonic and luminescent downshifting effects, Appl. Surf. Sci. 439 (2018) 868–875, http://dx.doi.org/10.1016/j.apsusc.2017.12.232.

[104] W.-J. Ho, J.-C. Chen, J.-J. Liu, C.-H. Ho, Enhancing luminescent down-shifting of Eu-doped phosphors by incorporating plasmonic silver nanoparticles for silicon solar cells, Appl. Surf. Sci. 532 (2020) 147434, http://dx.doi.org/10.1016/j.apsusc.2020.147434.

[105] W.-J. Ho, J.-J. Liu, J.-C. Chen, Characterization of plasmonic scattering, luminescent down-shifting, and metal-enhanced fluorescence and applications on silicon solar cells, Nanomaterials 11 (4) (2021) 1013, http://dx.doi.org/10.3390/nano11041013.

[106] J. Garcia, L. Bontempo, L. Gomez-Malagon, L. Kassab, Efficiency boost in Si-based solar cells using tellurite glass cover layer doped with Eu^{3+} and silver nanoparticles, Opt. Mater. 88 (2019) 155–160, http://dx.doi.org/10.1016/j.optmat.2018.11.028.

[107] S.-W. Lee, S. Kim, S. Bae, K. Cho, T. Chung, L.E. Mundt, S. Lee, S. Park, H. Park, M.C. Schubert, S.W. Glunz, Y. Ko, Y. Jun, Y. Kang, H.-S. Lee, D. Kim, UV degradation and recovery of perovskite solar cells, Sci. Rep. 6 (1) (2016) 38150, http://dx.doi.org/10.1038/srep38150.

[108] A. Sinha, J. Qian, S.L. Moffitt, K. Hurst, K. Terwilliger, D.C. Miller, L.T. Schelhas, P. Hacke, UV-induced degradation of high-efficiency silicon PV modules with different cell architectures, Prog. Photovolt., Res. Appl. 31 (1) (2023) 36–51, http://dx.doi.org/10.1002/pip.3606.

[109] N. Pinochet, R. Couderc, S. Therias, Solar cell UV-induced degradation or module discolouration: Between the devil and the deep yellow sea, Prog. Photovolt., Res. Appl. 31 (11) (2023) 1091–1100, http://dx.doi.org/10.1002/pip.3725.

[110] H. Hovel, R. Hodgson, J. Woodall, The effect of fluorescent wavelength shifting on solar cell spectral response, Sol. Energy Mater. 2 (1) (1979) 19–29, http://dx.doi.org/10.1016/0165-1633(79)90027-3.

[111] T. Trupke, M.A. Green, P. Würfel, Improving solar cell efficiencies by down-conversion of high-energy photons, J. Appl. Phys. 92 (3) (2002) 1668–1674, http://dx.doi.org/10.1063/1.1492021.

[112] E. Klampaftis, D. Ross, K.R. McIntosh, B.S. Richards, Enhancing the performance of solar cells via luminescent down-shifting of the incident spectrum: A review, Sol. Energy Mater. Sol. Cells 93 (8) (2009) 1182–1194, http://dx.doi.org/10.1016/j.solmat.2009.02.020.

[113] M. de la Mora, O. Amelines-Sarria, B. Monroy, C. Hernández-Pérez, J. Lugo, Materials for downconversion in solar cells: Perspectives and challenges, Sol. Energy Mater. Sol. Cells 165 (January) (2017) 59–71, http://dx.doi.org/10.1016/j.solmat.2017.02.016.

[114] N.S. Satpute, C.M. Mehare, A. Tiwari, H.C. Swart, S.J. Dhoble, Synthesis and luminescence characterization of downconversion and downshifting phosphor for efficiency enhancement of solar cells: Perspectives and challenges, ACS Appl. Electron. Mater. 4 (7) (2022) 3354–3391, http://dx.doi.org/10.1021/acsaelm.2c00595.

[115] D. Yu, T. Yu, H. Lin, S. Zhuang, D. Zhang, Recent advances in luminescent downconversion: New materials, techniques, and applications in solar cells, Adv. Opt. Mater. 10 (12) (2022) 2200014, http://dx.doi.org/10.1002/adom.202200014.

[116] R. Rothemund, Optical modelling of the external quantum efficiency of solar cells with luminescent down-shifting layers, Sol. Energy Mater. Sol. Cells 120 (PART B) (2014) 616–621, http://dx.doi.org/10.1016/j.solmat.2013.10.004.

[117] J. Keil, J.S. Silvia, D.M. Kroupa, V.E. Ferry, Optical coupling efficiency, photon loss, and efficiency estimates for c-Si PERC modules enhanced with downconverting films and nanocomposites, ACS Appl. Energy Mater. 6 (21) (2023) 10978–10986, http://dx.doi.org/10.1021/acsaem.3c01792.

[118] J. Xu, W. Pan, W. Shen, Efficiency enhancement of solar cell by using methylammonium lead tribromide/polymethyl methacrylate hybrid film as luminescent down shifting layer, Sol. Energy Mater. Sol. Cells 260 (2023) 112478, http://dx.doi.org/10.1016/j.solmat.2023.112478.

[119] R. Guerrero-Lemus, J. Sanchiz, M. Sierra, I.R. Martín, C. Hernández-Rodríguez, D. Borchert, Alternative and fully experimental procedure for characterizing down-shifters placed on photovoltaic devices, Sol. Energy Mater. Sol. Cells 185 (2018) 312–317, http://dx.doi.org/10.1016/j.solmat.2018.05.051.

[120] C. Yang, H.A. Atwater, M.A. Baldo, D. Baran, C.J. Barile, M.C. Barr, M. Bates, M.G. Bawendi, M.R. Bergren, B. Borhan, C.J. Brabec, S. Brovelli, V. Bulović, P. Ceroni, M.G. Debije, J.-M. Delgado-Sanchez, W.-J. Dong, P.M. Duxbury, R.C. Evans, S.R. Forrest, D.R. Gamelin, N.C. Giebink, X. Gong, G. Griffini, F. Guo, C.K. Herrera, A.W. Ho-Baillie, R.J. Holmes, S.-K. Hong, T. Kirchartz, B.G. Levine, H. Li, Y. Li, D. Liu, M.A. Loi, C.K. Luscombe, N.S. Makarov, F. Mateen, R. Mazzaro, H. McDaniel, M.D. McGehee, F. Meinardi, A. Menéndez-Velázquez, J. Min, D.B. Mitzi, M. Moemeni, J.H. Moon, A. Nattestad, M.K. Nazeeruddin, A.F. Nogueira, U.W. Paetzold, D.L. Patrick, A. Pucci, B.P. Rand, E. Reichmanis, B.S. Richards, J. Roncali, F. Rosei, T.W. Schmidt, F. So, C.-C. Tu, A. Vahdani, W.G. van Sark, R. Verduzco, A. Vomiero, W.W. Wong, K. Wu, H.-L. Yip, X. Zhang, H. Zhao, R.R. Lunt, Consensus statement: Standardized reporting of power-producing luminescent solar concentrator performance, Joule 6 (1) (2022) 8–15, http://dx.doi.org/10.1016/j.joule.2021.12.004.

[121] S. Pillai, M.A. Green, Plasmonics for photovoltaic applications, Sol. Energy Mater. Sol. Cells 94 (9) (2010) 1481–1486, http://dx.doi.org/10.1016/j.solmat.2010.02.046.

[122] Y.H. Jang, Y.J. Jang, S. Kim, L.N. Quan, K. Chung, D.H. Kim, Plasmonic solar cells: From rational design to mechanism overview, Chem. Rev. 116 (24) (2016) 14982–15034, http://dx.doi.org/10.1021/acs.chemrev.6b00302.

[123] Y.-F. Li, Z.-L. Kou, J. Feng, H.-B. Sun, Plasmon-enhanced organic and perovskite solar cells with metal nanoparticles, Nanophotonics 9 (10) (2020) 3111–3133, http://dx.doi.org/10.1515/nanoph-2020-0099.

[124] B. Ai, Z. Fan, Z.J. Wong, Plasmonic–perovskite solar cells, light emitters, and sensors, Microsyst. Nanoeng. 8 (1) (2022) 5, http://dx.doi.org/10.1038/s41378-021-00334-2.

[125] A. Bright (Ed.), Plasmonic interaction in enhanced luminescent down-shifting layers for photovoltaic devices, in: Plasmonics: Advances in Research and Applications, Nova Science Publishers, Inc, New York, 2017.

[126] J. Walshe, M. Girtan, S. McCormack, J. Doran, G. Amarandei, Combined experimental and modeling analysis for the development of optical materials suitable to enhance the implementation of plasmonic-enhanced luminescent down-shifting solutions on existing silicon-based photovoltaic devices, ACS Appl. Electron. Mater. 3 (6) (2021) 2512–2525, http://dx.doi.org/10.1021/acsaelm.1c00018.

[127] V.A. Markel, Introduction to the Maxwell Garnett approximation: tutorial, J. Opt. Soc. Amer. A 33 (7) (2016) 1244–1256, http://dx.doi.org/10.1364/JOSAA.33.001244.

[128] V.A. Markel, Maxwell Garnett approximation (advanced topics): tutorial, J. Opt. Soc. Amer. A 33 (11) (2016) 2237–2255, http://dx.doi.org/10.1364/JOSAA.33.002237.

[129] V.A. Markel, Maxwell Garnett approximation in random media: tutorial, J. Opt. Soc. Amer. A 39 (4) (2022) 535–544, http://dx.doi.org/10.1364/JOSAA.450850.

[130] M. Rafiee, S. Chandra, H. Ahmed, K. Barnham, S.J. McCormack, Small and large scale plasmonically enhanced luminescent solar concentrator for photovoltaic applications: Modelling optimisation and sensitivity analysis, Opt. Express 29 (10) (2021) 15031–15052, http://dx.doi.org/10.1364/OE.418183.

[131] J. Hu, Y. Yu, B. Jiao, S. Ning, H. Dong, X. Hou, Z. Zhang, Z. Wu, Realizing improved performance of down-conversion white organic light-emitting diodes by localized surface plasmon resonance effect of Ag nanoparticles, Organ. Electron. 31 (2016) 234–239, http://dx.doi.org/10.1016/j.orgel.2016.01.031.

[132] V.G. Kravets, A.V. Kabashin, W.L. Barnes, A.N. Grigorenko, Plasmonic surface lattice resonances: a review of properties and applications, Chem. Rev. 118 (12) (2018) 5912–5951, http://dx.doi.org/10.1021/acs.chemrev.8b00243.

[133] A.D. Utyushev, V.I. Zakomirnyi, I.L. Rasskazov, Collective lattice resonances: Plasmonics and beyond, Rev. Phys. 6 (2021) 100051, http://dx.doi.org/10.1016/j.revip.2021.100051.

[134] G. Vecchi, V. Giannini, J. Gómez Rivas, Shaping the fluorescent emission by lattice resonances in plasmonic crystals of nanoantennas, Phys. Rev. Lett. 102 (14) (2009) 146807, http://dx.doi.org/10.1103/PhysRevLett.102.146807.

[135] V.O. Byelobrov, T.M. Benson, A.I. Nosich, Binary grating of subwavelength silver and quantum wires as a photonic-plasmonic lasing platform with nanoscale elements, IEEE J. Sel. Top. Quantum Electron. 18 (6) (2012) 1839–1846, http://dx.doi.org/10.1109/JSTQE.2012.2213586.

[136] J.Y. Suh, C.H. Kim, W. Zhou, M.D. Huntington, D.T. Co, M.R. Wasielewski, T.W. Odom, Plasmonic bowtie nanolaser arrays, Nano Lett. 12 (11) (2012) 5769–5774, http://dx.doi.org/10.1021/nl303086r.

[137] F. van Beijnum, P.J. van Veldhoven, E.J. Geluk, M.J.A. de Dood, G.W. 't Hooft, M.P. van Exter, Surface plasmon lasing observed in metal hole arrays, Phys. Rev. Lett. 110 (20) (2013) 206802, http://dx.doi.org/10.1103/PhysRevLett.110.206802.

[138] D.G. Baranov, D.A. Zuev, S.I. Lepeshov, O.V. Kotov, A.E. Krasnok, A.B. Evlyukhin, B.N. Chichkov, All-dielectric nanophotonics: the quest for better materials and fabrication techniques, Optica 4 (7) (2017) 814–825, http://dx.doi.org/10.1364/OPTICA.4.000814.

[139] R. Heilmann, A.I. Väkeväinen, J.-P. Martikainen, P. Törmä, Strong coupling between organic dye molecules and lattice modes of a dielectric nanoparticle array, Nanophotonics 9 (2) (2020) 267–276, http://dx.doi.org/10.1515/nanoph-2019-0371.

[140] S. Murai, G.W. Castellanos, T.V. Raziman, A.G. Curto, J.G. Rivas, Enhanced light emission by magnetic and electric resonances in dielectric metasurfaces, Adv. Opt. Mater. 8 (16) (2020) 1902024, http://dx.doi.org/10.1002/adom.201902024.

[141] V. Rutckaia, F. Heyroth, G. Schmidt, A. Novikov, M. Shaleev, R.S. Savelev, J. Schilling, M. Petrov, Coupling of germanium quantum dots with collective sub-radiant modes of silicon nanopillar arrays, ACS Photon. 8 (1) (2021) 209–217, http://dx.doi.org/10.1021/acsphotonics.0c01319.

[142] M. Higashino, S. Murai, T.-Y. Lo, S. Tomita, K. Tanaka, Photoluminescence coupled to electric and magnetic surface lattice resonance in periodic arrays of zirconia nanoparticles, J. Mater. Chem. C 10 (26) (2022) 9730–9739, http://dx.doi.org/10.1039/D2TC01119K.

[143] V.I. Zakomirnyi, A. Moroz, R. Bhargava, I.L. Rasskazov, Large fluorescence enhancement via lossless all-dielectric spherical mesocavities, ACS Nano 18 (2) (2024) 1621–1628, http://dx.doi.org/10.1021/acsnano.3c09777.

[144] C. Gong, W. Liu, N. He, H. Dong, Y. Jin, S. He, Upconversion enhancement by a dual-resonance all-dielectric metasurface, Nanoscale 11 (4) (2019) 1856–1862, http://dx.doi.org/10.1039/C8NR08653B.

[145] Y. Liu, A. Teitelboim, A. Fernandez-Bravo, K. Yao, M.V.P. Altoe, S. Aloni, C. Zhang, B.E. Cohen, P.J. Schuck, E.M. Chan, Controlled assembly of upconverting nanoparticles for low-threshold microlasers and their imaging in scattering media, ACS Nano 14 (2) (2020) 1508–1519, http://dx.doi.org/10.1021/acsnano.9b06102.